A novel reinforced-concrete buckling-restrained brace for precast concrete lateral-load-resisting frames

Shane Oh, Yahya C. Kurama, Jon Mohle, Lily Polster, Mark Manning, and Brad D. Weldon

Buckling-restrained braces are a type of axial structural component used primarily for lateral strength and stiffness of steel building structures in seismic regions. These braces are typically composed of a high-ductility steel core plate (also known as the yielding core) that is surrounded by but axially decoupled from a grout-filled steel tube. Under compressive axial loading, the grout-filled tube prevents buckling of the yielding core such that the behavior and design of the brace in compression are dictated primarily by the material strength of the steel core rather than its buckling load.[1–5] Subsequently, the hysteretic axial load-deformation behavior of a buckling-restrained brace is nearly symmetric, with large energy dissipation across tension and compression cycles.

Most commonly, buckling-restrained braces are configured as diagonal components within a lateral-load-resisting building frame, similar to other braced-frame building systems, such as concentrically braced frames. When properly designed and detailed, buckling-restrained braced frames perform exceptionally well relative to other braced systems because they concentrate stable nonlinear behavior within the yielding regions of the brace while maintaining elasticity in the other frame components.[3,6–9] These findings have led to the codification of steel buckling-restrained braced building frames with the largest seismic response modification coefficient R (equal to 8) allowed in the United States, starting in the 2005 edition of the American Society of Civil Engineers' *Minimum Design Loads for Buildings and Other Structures* (ASCE 7-05).[10] Subsequently, buckling-restrained braced frames have become the lateral system of choice for

- This paper describes a numerical investigation on the seismic design and behavior of a novel reinforced-concrete buckling-restrained brace component for use in precast concrete lateral-load-resisting frames.

- Nonlinear finite element analyses were conducted to investigate the following potential undesirable failure modes of the brace: global buckling of the brace, closure of the end gaps, and local translational buckling of the energy-dissipation bars over the end gaps.

- The results indicated that failure through global buckling is unlikely for practical brace designs; however, axially decoupled shear dowels may be needed to prevent local buckling of the energy-dissipation bars.

steel building structures because they have been associated with reduced costs and improved ductile performance.

Previous research on the use of buckling-restrained braces in precast concrete construction has investigated nonbuilding structures (specifically, bridge bents) and retrofit applications.[11–14] Despite their popularity in steel buildings, buckling-restrained braced frame systems have rarely been incorporated as the primary lateral-load-resisting system in new concrete building construction, largely because research on these systems is limited. Currently, only one precast concrete building in the United States has implemented steel buckling-restrained braces.[15] To continue exploring and developing the potential advantages of buckling-restrained braced frames for precast concrete structures, this paper introduces and numerically evaluates a novel reinforced-concrete brace component specifically suited for precast concrete construction.

Previous research

One pertinent research study of precast concrete building structures with buckling-restrained braces was conducted by Guerrero et al.[16] This investigation compared the dynamic properties and seismic responses of two 4-story frame specimens designed under Mexican building practices by testing frames with and without steel buckling-restrained braces on a shake table. The tests demonstrated that buckling-restrained braces improve the seismic behavior of precast concrete building frames by reducing damage in the beam and column components and joints.

A recent numerical study[17] evaluated the seismic design of precast concrete building frames with steel buckling-restrained braces based on the methodology set forth in the Federal Emergency Management Agency's *Quantification of Building Seismic Performance Factors* (FEMA P-695).[18] A set of 32 archetype precast concrete braced frames covering a wide range of parameters (such as 2- to 9-story buildings and different brace configurations) were designed using the equivalent lateral force procedure,[10] consistent with current U.S. building code requirements. Nonlinear static pushover analyses and incremental dynamic analyses[19] of the archetype frames were conducted and validated with the available shake-table test data.[16] The results of the FEMA P-695 analyses of the archetypes supported a seismic response modification coefficient R of 8, the same value currently in use for buckling-restrained braced frames in steel buildings. The results from this numerical work indicated the potential benefits of precast concrete buckling-restrained braced frames for new building construction and the need for further research in this area of investigation.

In another recent study, Kessler tested the welded gusset plate connection between a steel buckling-restrained brace (which was simulated using a hydraulic actuator) and the beam and column components of a precast concrete building frame.[20] The test results showed that the gusset plate forces varied significantly from the forces predicted by the American Institute of Steel Construction's (AISC's) uniform force method for the seismic design of buckling-restrained braced connections in steel building frames.[21] Practical challenges of incorporating steel braces in precast concrete construction were also identified through this research. Specifically, the misalignment of an embedded plate in the corbel required the welded connection of the gusset plate to the corbel to be redesigned.

Research goals, contributions, and scope

The research described in this paper focuses on the development of a novel ductile yielding brace that can be produced as an integrated structural component of an efficient, all–precast concrete buckling-restrained braced frame unit. This precast concrete braced-frame unit is intended to be produced flat at a precast concrete plant, transported to the construction site, and then stacked upright with grouted seismic dowel splices at each floor level, similar to the production, transportation, and erection of a multipanel precast concrete structural wall.

Figure 1 shows a single-story precast concrete frame unit with two of the proposed reinforced-concrete brace components used in a chevron configuration. Depending on the frame dimensions, this concept may also be used in a single-diagonal brace configuration or in a two-story braced-frame unit.

As described in the "Description and Design of the Novel Reinforced Concrete Bucking-Restrained Brace" section of this paper, the proposed brace uses ASTM A706[22] reinforcement as yielding energy-dissipation steel inside confinement hoops, including a wrapped (unbonded) stretch length for the bars to yield in tension without fracture. In addition, a small gap is located at each end of the brace to allow the bars to yield in compression without the brace concrete coming into contact with the beam and column components.

The envisioned advantages of this all–precast concrete buckling-restrained braced frame system are as follows:

- improved cost effectiveness through single-trade (all–precast concrete) design and construction

- elimination of welded/embedded steel plate connections to the precast concrete beams and columns

- ability to customize the brace details (such as length and cross section) at the precast concrete plant together with the rest of the frame unit

Although commercial steel buckling-restrained braces can be used in a precast concrete building frame, experimental research[20] and the previous application[15] of steel braces in a precast concrete building in the New Madrid seismic zone in the central United States have shown that there may be practical challenges and increased costs in implementing steel braces in a precast concrete structure. The higher costs are associated with the welded and embedded steel plate
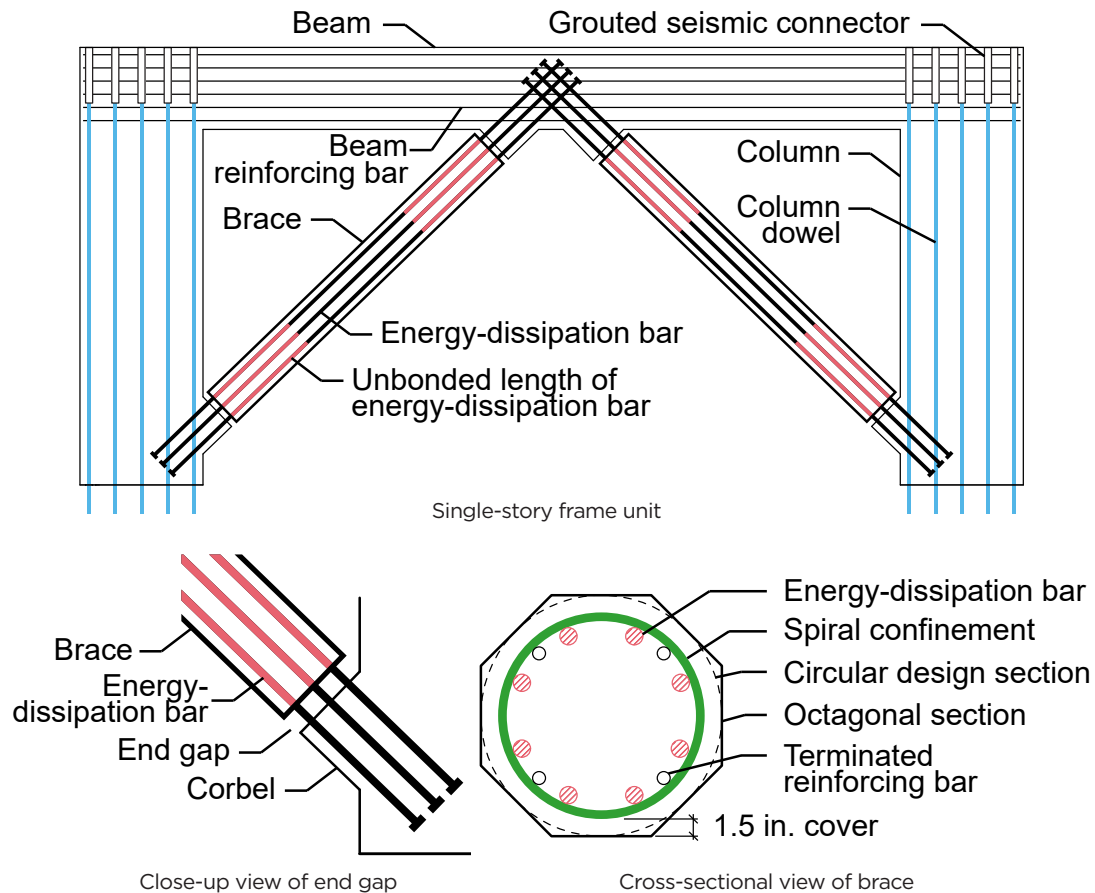
Figure 1. Potential use of novel precast concrete buckling-restrained braces in chevron configuration within a single-story precast concrete frame unit (additional column, beam, and brace reinforcement are not shown for clarity). Note: 1 in. = 25.4 mm.

connections for steel braces, the differences in construction tolerances between steel and precast concrete, and the differences between the governing building code requirements for the steel braces and the code requirements for the rest of the frame. Furthermore, steel braces require custom fabrication in a facility separate from the precast concrete plant, resulting in logistical inefficiencies. In comparison, the proposed reinforced-concrete braces will be fully integrated into the initial design, detailing, and production of the precast concrete frame components.

This paper introduces the structural details and intended behavior of the proposed brace, provides a procedure for its design, describes a numerical evaluation of some of its potential failure modes, and makes recommendations for future numerical and experimental research. Because this investigation is the first study of this novel brace, the numerical analyses are focused on the isolated behavior of a single diagonal brace rather than its ultimate use within a frame. This limit in scope aims to allow the results from the numerical analyses to be affected only by the brace, without influence from the surrounding beam and column components, so that the brace behavior can be more directly studied.

A reinforced-concrete finite element analysis (FEA) software[23] was used to conduct the numerical analyses, which investigated selected structural performance limits (failure modes) of the novel brace. This numerical study did not include all potential failure modes of the proposed brace. Post-earthquake repair or replacement was also not within the scope of this research. Furthermore, the results from the analyses are currently not validated by experimental data. Ultimately, the analysis results presented in the paper are intended to provide guidance for future experimental research, especially with respect to behaviors and failure modes that are difficult to simulate numerically, as well as for future numerical research, especially with respect to the behavior of precast concrete braced-frame subassemblies and multistory structures.

Description and design of the novel reinforced-concrete buckling-restrained brace

This section outlines the characteristics of the reinforced-concrete buckling-restrained brace, including a proposed procedure for its design. Where applicable, code requirements from the American Concrete Institute's *Building Code*

Requirements for Structural Concrete (ACI 318-19) and Commentary (ACI 318R-19)[24] are adapted. Where no code specifications are applicable to the novel brace, some components of the design procedure are based on reasonable assumptions and limitations of the expected brace behavior.

Overview of the brace

The axial stiffness, strength, and ductility of the concrete brace are intended to be primarily governed by the axial, cyclic tension-compression behavior of ASTM A706[22] reinforcement (Fig. 1) as yielding energy-dissipation steel. Under cyclic loads, these energy-dissipation bars are designed to deform almost uniformly in compression and tension within a predetermined, unbonded length at each end of the brace (Fig. 1), providing axial stiffness, strength, and ductility for the brace. The unbonded length at each end of the brace includes the gap region in addition to a region over which the bars are wrapped in plastic sheeting to ensure axial separation of the bars from the concrete; this design has been successfully applied in precast concrete special moment-resisting frames and structural walls.[25,26] Under tensile loading of the brace, the axial deformations of the energy-dissipation bars are nearly uniformly distributed over the unbonded length at each end, thus allowing the brace to reach large story drifts without bar fracture. Under compressive loads, the confined concrete of the brace prevents the energy-dissipation bars from buckling over the unbonded length, allowing the bars to reach their full material strength.

During the production of the braced-frame unit (Fig. 1) at the precast concrete plant, a small gap with a predetermined width (a few inches) is formed at each end of the brace. These gaps allow the energy-dissipation bars to compress freely when the brace is in compression without the brace concrete contacting the column and beam corbel zones. This detail minimizes compression damage to the brace and the corbels, and it ensures that the axial tension-compression behavior of the brace is nearly symmetrical, as governed primarily by the yielding of the energy-dissipation bars. The gap width at each end of the brace is designed to be large enough to prevent concrete bearing over the expected deformation of the brace in compression while also small enough to prevent the energy-dissipation bars from buckling within this region (where the bars are not laterally supported). While the brace could feasibly be built with a single unbonded region and corresponding gap at one end, designing unbonded and gap regions at both ends of the brace allows the total required gap width to be equally distributed between the two ends, thereby minimizing the potential for buckling of the energy-dissipation bars.

The ends of the energy-dissipation bars are embedded and anchored through the corbel regions and into the column and beam concrete of the precast concrete frame. The corbel regions are necessary to ensure direct axial-load transfer from the brace to the frame and to minimize the possibility of shear slip at the brace-to-frame interfaces. Headed anchorages are designed per ACI 318-19 for the ends of the energy-dissipation bars to reduce the required development lengths and minimize complexities with the detailing of the reinforcement inside the braced frame. For typical beam, column, and corbel dimensions, this detail provides adequate anchorage to develop the ends of the energy-dissipation bars.

The midlength bonded regions of the energy-dissipation bars (brace length between the two unbonded regions) are designed to remain linearly elastic during the compressive and tensile axial deformations of the brace. This behavior is achieved by bonding the energy-dissipation bars to the surrounding concrete over the midlength of the brace. To ensure that the bars remain bonded while the brace is in tension, this region is designed to provide at least twice the development length for the bars per ACI 318-19 (that is, the full development length is provided extending from each unbonded region to the midlength of the brace).

Furthermore, additional bonded longitudinal reinforcement is placed over the entire length of the brace from end gap to end gap to prevent yielding of the energy-dissipation bars over the bonded midlength region of the brace and to provide additional confinement of the brace concrete, together with transverse confinement reinforcement. Because the additional bonded longitudinal reinforcement does not cross the end gaps of the brace (that is, the additional bars are terminated at each end of the brace), the axial stiffness, strength, and ductility of the brace are governed primarily by the energy-dissipation bars crossing the end gaps. This additional longitudinal reinforcement in the brace is referred to as *terminated* longitudinal reinforcement throughout the remainder of this paper.

As the brace undergoes axial tensile deformations, large post-yield tensile stresses are expected to develop in the unbonded regions of the energy-dissipation bars. However, in the bonded region within the midlength of the brace, the tension force in the brace is shared between the energy-dissipation bars and the terminated bars. As tensile stresses are transferred from the energy-dissipation bars to the terminated bars, concrete cracking develops in the bonded region of the brace. To limit the width of these cracks so that the largest tensile deformations occur at the end gaps rather than within the brace, the terminated reinforcement is designed to remain essentially linearly elastic. This is also necessary for the energy-dissipation bars to remain linearly elastic in the bonded regions. As such, the axial stiffness of the brace within the bonded midlength region is governed by the elastic stiffness of the total area of the longitudinal steel (that is, the total area of the energy-dissipation and terminated bars), while the stiffness of the unbonded region is governed by the smaller stiffness of the energy-dissipation bars alone. As yielding develops in the unbonded regions of the energy-dissipation bars, the tensile deformations of the brace are further concentrated within the end gaps of the brace. Due to the cracking of the concrete, the brace is expected to be less stiff in tension compared with the stiffness in compression. Under reversed cyclic loading, the opening and closing of these cracks result

in slightly asymmetric behavior in tension and compression; however, the effect of this asymmetry is not significant to the overall behavior, as demonstrated in the analyses described later in this paper.

Design procedure

Figure 2 presents the design steps, which are described in more detail herein. The first design step is to determine the factored design axial force of the brace N_u following the ASCE 7-22[27] equivalent lateral force procedure. Because the scope of this paper is limited to isolated brace behavior, the design procedure described herein does not include a full frame design with subsequent calculation of the brace design forces. However, the procedure for calculating the design axial forces for the proposed brace is identical to the procedure used to determine the design axial forces for steel buckling-restrained braces (Oh et al.[17] provides more details about this calculation).

The factored design axial force N_u is used to determine the total required area of the energy-dissipation bars following the area-based approach typically used to determine the yielding core plate area in steel buckling-restrained braces (AISC's *Seismic Design Manual*[28] or Oh et al.[17]). In this approach, the required area of the energy-dissipation bars is found based on the lowest expected steel yield strength $f_{y,min}$. Using a capacity reduction factor for axial strength ϕ of 0.9, the minimum required area of the energy-dissipation bars $A_{b,min}$ is calculated as $N_u/(\phi f_{y,min})$. The capacity reduction factor is intended to ensure that the brace has sufficient capacity to meet the design axial force, similar to the strength design of steel buckling-restrained braces.[28]

Next, the size and number of the energy-dissipation bars are chosen to meet the minimum area requirement. Per ACI 318-19 section 25.4.4.1, the size of the energy-dissipation bars is limited to no. 11 (36M) or smaller for headed bars. To protect against buckling of the energy-dissipation bars and also minimize congestion, a smaller number of larger-size bars (not to exceed no. 11) are chosen rather than a larger number of smaller-size bars.

In this research, the total area of the terminated longitudinal reinforcement was designed to be approximately 30% of the total provided energy-dissipation bar area. As stated previously, the design intent is to allow the energy-dissipation bars and the terminated bars to share the total axial force in the bonded region of the brace such that the reinforcement in the bonded region does not yield even when the unbonded regions of the energy-dissipation bars have attained significant post-yield strains. In other words, the total yield strength of the steel within the bonded length of the brace is at least equal to the maximum (ultimate) axial force that is expected in the brace. The distribution of stresses from the energy-dissipation bars to the terminated bars within the bonded region of the brace requires effective development of the bars, which should be validated in future experimental research.
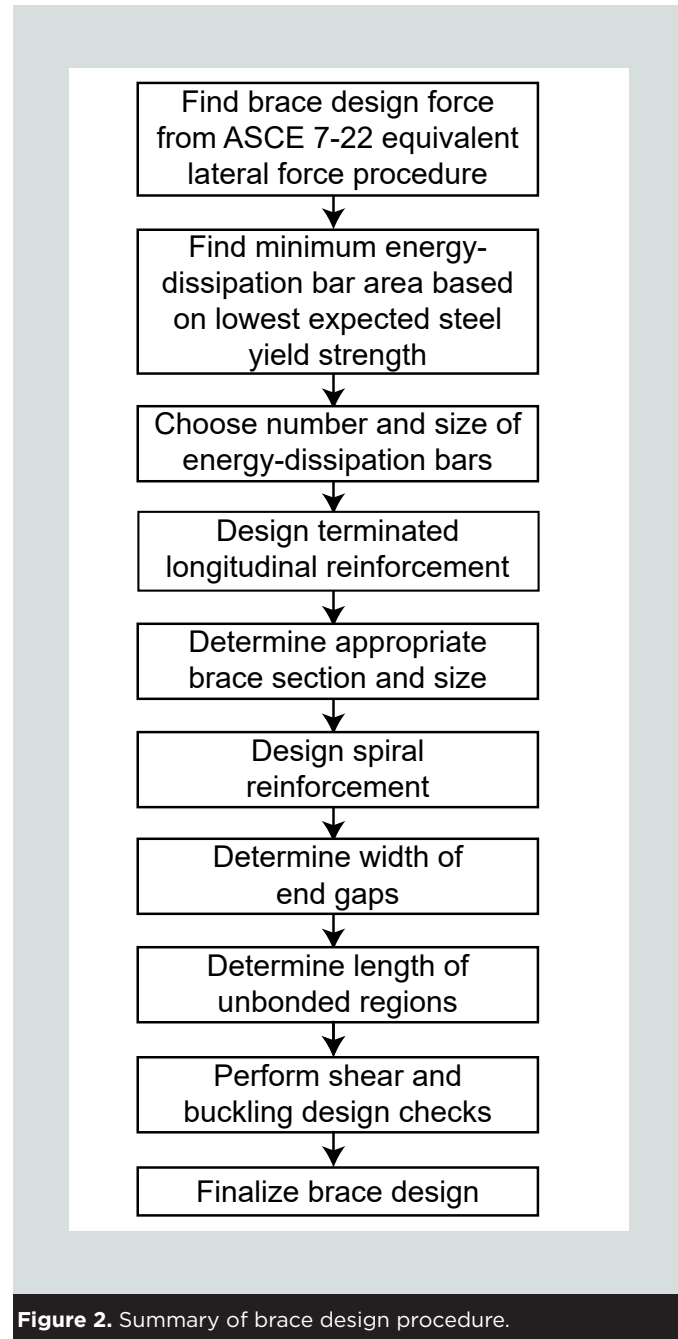
Figure 2. Summary of brace design procedure.

Once the areas of the energy-dissipation bars and terminated bars are determined, several simplifying assumptions are made to design the reinforced-concrete brace section. While a square or rectangular brace cross section can be used, the brace design in this study initially assumed a circular section, with the energy-dissipation bars arranged in a circular pattern (Fig. 1) and spiral reinforcement to provide concrete confinement. At the end of the design process, the circularly designed section was adjusted into an octagonal shape, thus creating flat surfaces to simplify the horizontal casting process of the precast concrete while retaining the benefits of a circular reinforcement layout.

Because the concrete section of the brace is not used to develop the brace's axial strength, the gross sectional area is determined to minimize the concrete volume without rein-

forcement congestion, typically targeting a total longitudinal reinforcement ratio (including both the energy-dissipation bars and the terminated bars) of no more than 6% of the gross concrete brace area. This upper limit was chosen based on the maximum reinforcement ratio allowed for columns of special reinforced-concrete frames in section 18.7.4 of ACI 318-19.

More efficient (that is, smaller) concrete sections would be possible if a higher total reinforcement ratio could be used in the brace design. Specifically, section 10.6 of ACI 318-19 permits a maximum total reinforcement ratio of 8%. The transverse shear and confinement reinforcement for buckling-restrained braces is expected to be less congested compared with columns in special reinforced-concrete frames (because of nearly uniaxial loading of the brace concrete rather than combined large axial, shear, and bending forces in columns); therefore, simpler reinforcement detailing may permit this higher maximum reinforcement ratio of 8%. The numerical parametric study described in later sections of this paper investigates the effect of the percentage of energy-dissipation bar reinforcement on the brace behavior. However, future experimental research is necessary in this area.

The terminated bars are placed evenly against the spiral reinforcement between the energy-dissipation bars, with a clear cover of 1.5 in. (38 mm) provided outside the spiral reinforcement (Fig. 1). Given the novel nature of the brace, no current code requirement is directly applicable to the design of the spiral reinforcement. As such, the brace designs described in this paper followed the requirements of ACI 318-19 section 18.7.5 to determine the spiral reinforcement ratio.

The next design steps are to determine the width of the end gaps of the brace and the length of the unbonded regions of the energy-dissipation bars. These dimensions are designed based on a maximum design story drift $\pm\Delta_{d,max}$ under an extreme earthquake event that may be anticipated at the building site.

The gap widths at the brace ends are designed to be large enough to prevent closure in compression at the maximum design story drift $\Delta_{d,max}$. This width is determined by calculating the change in brace length Δ_b at the maximum design story drift $\Delta_{d,max}$ as follows:

$$\Delta_b = \sqrt{h^2 + \left(w + \Delta_{d,max}h\right)^2} - \ell_b$$

where

h = work point–to–work point height of the brace, where the work points are located at the intersections of the brace centerline with the centerlines of the beam and column components of the frame

w = work point–to–work point horizontal length of the brace

ℓ_b = work point–to–work point diagonal length of the brace

As described by Kersting et al.[29] and depicted in **Fig. 3**, the equation to calculate Δ_b conservatively ignores axial deformations in the beam and column components, adopting a simplified shear frame model. Assuming that all axial deformations in the brace occur equally within the end gaps, the minimum width of each end gap $w_{g,min}$ is then calculated as $0.5\Delta_b$.

The required minimum unbonded length at each end of the brace is determined by ensuring that the maximum tensile strain of the energy-dissipation bars does not exceed the usable tensile strain limit $\varepsilon_{s,max}$ to prevent low-cycle fatigue fracture of the bars under cyclic loading. To determine this length, the brace axial deformation in tension at the maximum design story drift $\Delta_{d,max}$ is taken to be the same as that in compression, calculated as Δ_b previously. Assuming that all of this brace elongation occurs equally within the unbonded lengths of the energy-dissipation bars, the minimum unbonded length at each end of the brace $\ell_{unb,min}$ is then calculated as $0.5\Delta_b/\varepsilon_{s,max}$. In this approach, the total unbonded length of the energy-dissipation bars is split evenly between the two ends of the brace, similar to the even application of the two end gap widths. The unbonded lengths must be checked to ensure that sufficient development lengths remain in the middle bonded and end regions of the energy-dissipation bars.

For the braces analyzed in this research, the gap width and unbonded length dimensions were designed based on an assumed maximum design story drift $\Delta_{d,max}$ of ±4%. Furthermore, based on the cyclic testing of energy-dissipation bars by Aragon et al.,[30] a maximum tensile strain limit $\varepsilon_{s,max}$ of 0.06 was taken as the usable tensile strain limit for the bars under cyclic loading.

Additional design checks are necessary to ensure that global buckling of the brace and local buckling of the energy-dissipation bars (over the end gaps where the bars are not laterally supported) do not occur when the brace reaches the maximum design story drift $\Delta_{d,max}$ in compression. Design guidelines to
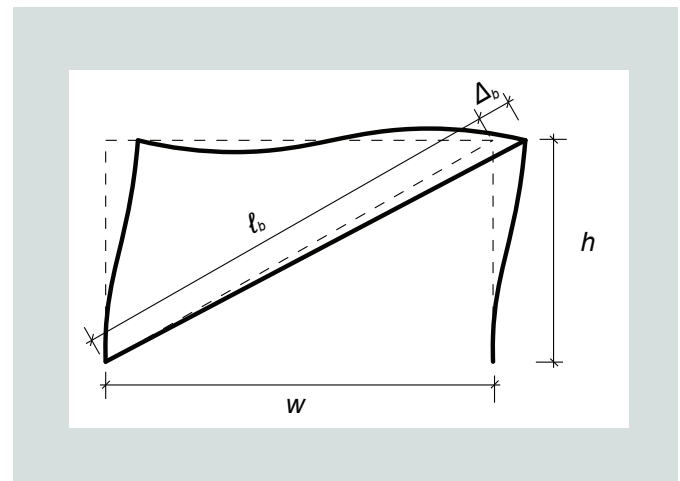
Figure 3. Idealized shear frame model for calculation of brace deformations. Source: Adapted from Kersting et al. Note: h = work point–to–work point height of brace; ℓ_b = work point–to–work point diagonal length of brace; w = work point–to–work point horizontal length of brace; Δ_b = change in brace length at maximum design story drift.

prevent these failure modes are described later in this paper. The brace section should also be checked for shear strength; however, the maximum shear forces in buckling-restrained braces are typically small.[17] Thus, this design check is not likely to be critical.

Finite element analysis and modeling

Finite element analyses were conducted to investigate the nonlinear behavior of the novel reinforced concrete brace. The purpose of these analyses was to evaluate the proposed design procedure and investigate some of the potential failure modes of the brace. Prototypical braces were designed using the upper limit of the factored design axial force N_u determined from the range of design forces for the archetype precast concrete frames with steel buckling-restrained braces reported in Oh et al.[17] This upper-limit design force of approximately 1200 kip (5300 kN) was chosen to ensure that the concrete braces designed in this research can provide similar maximum forces as the steel braces investigated in the previous study.

In addition to the analyses of the prototypical braces, analyses were also conducted on extreme brace configurations that are outside of the likely range of practicality. These braces were not meant to represent potential brace designs, but they were analyzed to gain a greater understanding of brace failure due to global buckling.

While a brace placed diagonally within a frame would predominantly undergo axial tension and compression deformations, it would also experience rotation under lateral interstory drift. **Figure 4** shows the isolated brace subassembly model that was used to investigate this axial-flexural brace behavior. In this model, a single diagonal brace is connected to an elastic concrete end block at the bottom end and a single-story elastic concrete column at the top end, while other components of the precast concrete frame (that is, beams, multistory columns, and beam-column joints) are excluded. The top surfaces of the bottom end block and column are free, while the bottom surface of the end block is fixed and the bottom of the column is pinned. The analyses were conducted by applying a pseudostatic, monotonic or reversed cyclic, lateral displacement at the work point located at the top of the column, thereby inducing interstory drift deformations to the brace.

The simplifications (for example, lack of other frame components) in this brace subassembly model result in small discrepancies with respect to the end boundary conditions of a brace within a multistory frame structure. However, these simplifications are conservative for the purposes of the failure analyses described in this paper, as almost all of the applied lateral load is carried by the brace (because the column base is pinned) while bending effects on the brace due to the rotation of the column are maximized (because the base of the bottom end block is fixed). Evidence supporting the conservative nature of these simplified boundary conditions for the brace is provided in the Simplifying Assumptions section of this paper.

Failure modes and analysis types

The following brace failure modes were investigated in this numerical study:
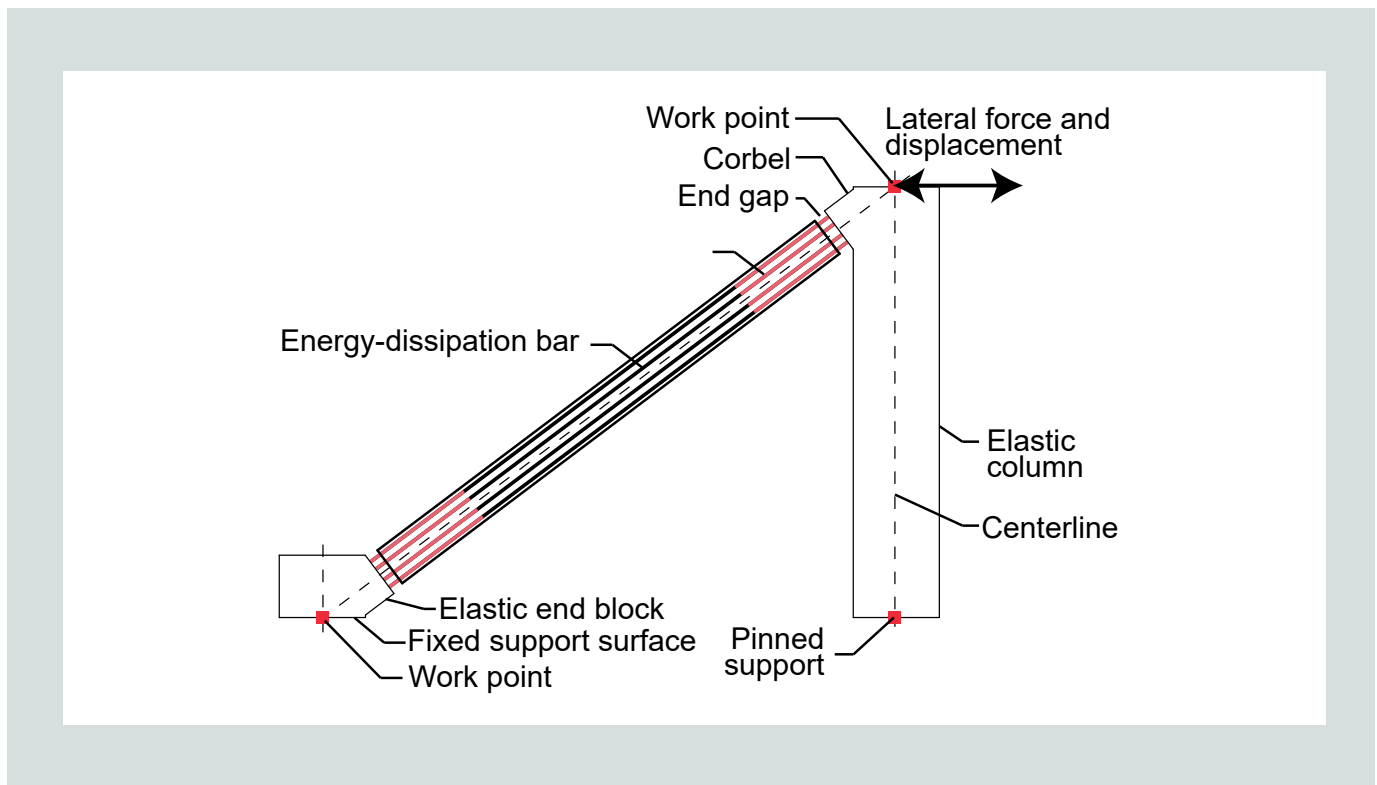

Figure 4. Brace subassembly modeled in the finite element analysis software.

- global buckling of the brace

- closure of the end gaps

- translational buckling of the energy-dissipation bars

Three types of lateral load analyses were conducted: monotonic compression analyses to investigate global buckling of the brace as well as closure of the end gaps; single-cyclic tension-compression analyses to investigate buckling of the energy-dissipation bars; and multicyclic tension-compression analyses to determine the intended full hysteretic behavior of a well-designed brace up to ductile low-cycle fatigue fracture of the energy-dissipation bars.

Table 1 presents a summary of these models, which are described in detail in the following sections. All analyses were conducted in displacement control by horizontally displacing the upper work point of the brace (Fig. 4) in increments of 0.04 in. (1 mm). For most of the analyses, this displacement increment corresponded to less than 0.1% of the unbonded length of the brace.

Other failure modes can also limit the behavior of the proposed brace. These other failure modes, which were not investigated in this study, include bond failure of the energy-dissipation bars and the terminated bars, yielding of bars within the bonded regions of the brace, and torsional buckling of the energy-dissipation bars crossing the end gaps. Experimental research is recommended to investigate these failure modes.

Modeling of the energy-dissipation bars in the bonded regions

Modeling of the energy-dissipation bars was separated into the unbonded regions at the ends of the brace and the bonded middle region (Fig. 4). To improve computational efficiency, the other bonded regions of the energy-dissipation bars within the elastic end block and column (across from the gap at each end of the brace) were not modeled explicitly. Instead, the ends of each energy-dissipation bar were assumed to be fixed to the elastic end block and column corbel face across from each gap. Bond slip and debonding of the bars in the bonded regions were not considered in the models; these undesirable behaviors require experimental investigation in future research.

The bonded length within the middle region of each energy-dissipation bar was modeled using discrete one-dimensional uniaxial truss (line) elements, with each truss element node "embedded" (constrained) to the surrounding concrete nodes, assuming perfect bond provided by adequate development lengths. Each truss element was assigned a bilinear reinforcing steel stress-strain $\sigma_s - \varepsilon_s$ relationship, with modulus of elasticity E_s of 29,000 ksi (200,000 MPa) and postyield strain-hardening modulus E_{sh} of 350 ksi (2400 MPa) for Grade 60 (414 MPa) steel and 500 ksi (3450 MPa) for Grade 80 (552 MPa) steel (**Fig. 5**). The cyclic stress-strain behavior of the bars was simulated using the default parameters for the Menegotto-Pinto reinforcing steel model in the finite element modeling software (Fig. 5).[23]

Modeling of the energy-dissipation bars in the unbonded regions

The behavior of the energy-dissipation bars in the unbonded regions governs the brace stiffness, strength, and ductility, representing the most critical aspects of the brace behavior and performance. As such, significant attention was given to the modeling of the bars and brace in these regions. Owing to limitations in the finite element modeling software, different methods were used to model the energy-dissipation bars based on the loading type (monotonic/single-cyclic versus multicyclic loading) to better investigate the different potential failure mechanisms.

For the monotonic compression analyses used to investigate global brace buckling and end-gap closure, the unbonded lengths of the energy-dissipation bars were modeled using three-dimensional 10-node quadratic tetrahedral elements.[23] Each energy-dissipation bar was simplified to a regular hexagonal cross section with area equal to the corresponding nominal bar area. A bilinear reinforcing steel stress-strain material was assigned to each element, using Von Mises plasticity for the yield condition and steel properties matching those for the material used for the one-dimensional bar elements described previously (Fig. 5). As shown in **Figure 6**, the ends of each unbonded region were fixed to the face of the corbel (corbel at top of pin-based column is shown, with similar details used for the bottom end-block corbel) and to the transition surface between the unbonded and bonded regions of the brace.

Table 1. Numerical models used in investigation of brace failure modes and behavior		
Failure mode and behavior	**Loading**	**Unbonded region of energy-dissipation bars**
Global buckling of brace	Monotonic compression	Three-dimensional elements
Closure of brace end gaps	Monotonic compression	
Buckling of energy-dissipation bars	Single cyclic	
Desired brace behavior up to ductile low-cycle fatigue fracture of energy-dissipation bars	Multicyclic	One- and three-dimensional elements in parallel
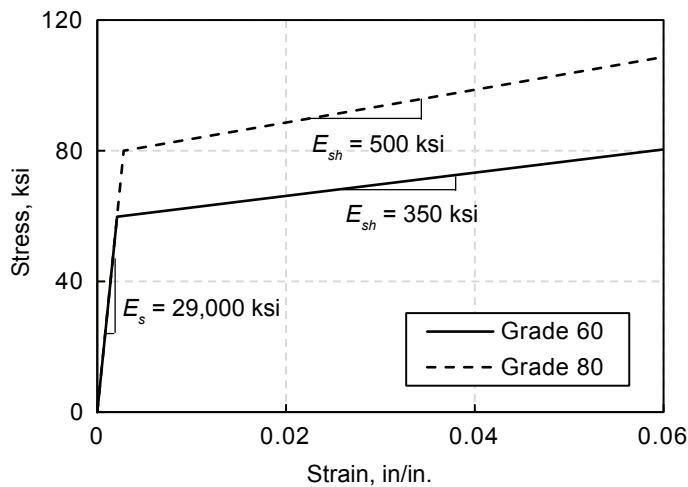
Monotonic steel stress-strain behavior (one-dimensional and three-dimensional elements)
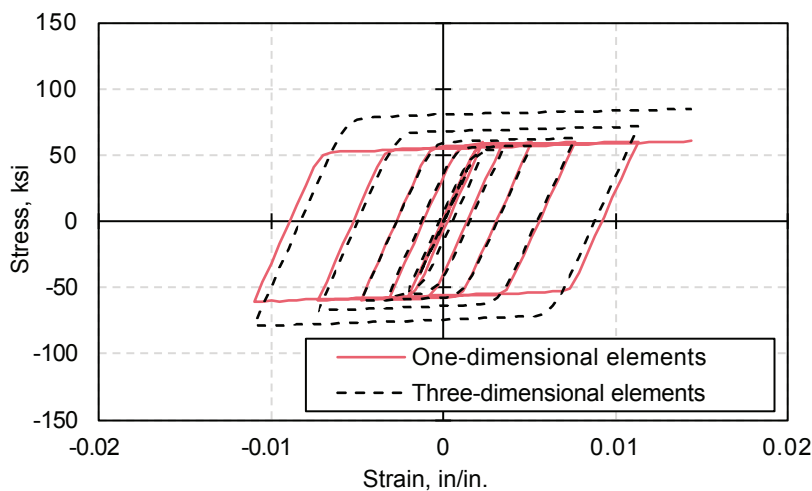
Cyclic steel stress-strain behavior

Figure 5. Stress-strain relationships for one-dimensional truss (line) and three-dimensional steel elements in the finite element analysis modeling software. Note: 1 in. = 25.4 mm; 1 ksi = 6.895 MPa; Grade 60 = 414 MPa; Grade 80 = 552 MPa.

To model the contact between the energy-dissipation bars and the brace concrete, each bar was encased in zero-thickness contact elements with interface contact and friction material properties. This material is based on the Mohr-Coulomb criterion using tension cutoff with user-defined cohesion and friction.[23] Because the energy-dissipation bars in the unbonded regions of the brace would be wrapped inside plastic sheeting, cohesion and friction between the bars and the surrounding concrete were assumed to be small and were neglected. The interface was assigned a large normal stiffness in compression but no strength in tension, modeling the contact between the bars and the concrete while also allowing for potential separation or splitting of the cover concrete from the bar.

Three-dimensional steel elements were also used in the single-cyclic tension-compression analyses to investigate energy-dissipation bar buckling. However, the cyclic stress-strain behavior of the three-dimensional steel elements in the finite element modeling software[23] exhibited an unrealistically high level of isotropic strain hardening (Fig. 5). Thus, an intentionally lowered initial yield strength was assigned to the three-dimensional steel elements in the single-cyclic analyses such that appropriate bar stresses developed after load reversal from tension into compression when modeling the buckling of the bars. This adjustment is discussed in more detail later in this paper.

It was not possible to take a similar approach to overcome the excessive isotropic strain hardening of the three-dimensional steel elements when conducting multicyclic analyses. Thus, in these analyses, each bar was modeled using one-dimensional uniaxial truss elements and three-dimensional tetrahedral elements in parallel (Fig. 6 multicyclic model). For each bar, these parallel one-dimensional and three-dimensional components separately simulated the axial and transverse behaviors of the bar, respectively, while ignoring the
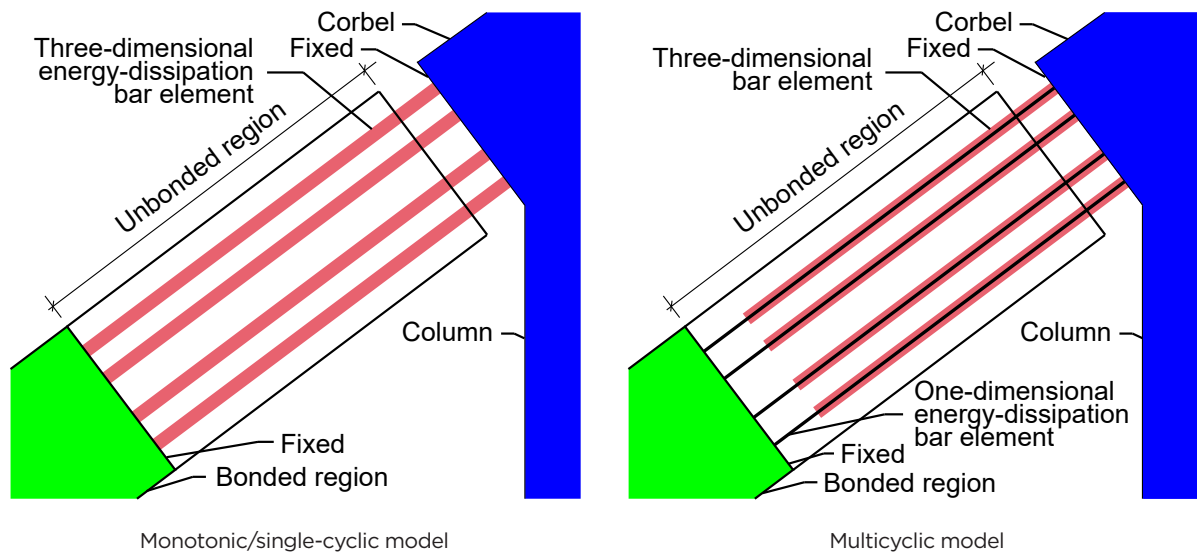
Figure 6. Modeling of energy-dissipation bars in unbonded regions of the brace for monotonic/single-cyclic analyses and multicyclic analyses.

interaction between the axial behavior and the flexural-shear behavior of the bar. The one-dimensional component with truss elements extended from the corbel face to the bonded region inside the brace. This component was assigned zero bond strength to allow the energy-dissipation bar to freely slide tangentially over the unbonded length while carrying axial forces.

Dowel effects from the transverse bending and shear deformations of the bar on the surrounding brace concrete were simulated by the second component, which had a hexagonal cross section using three-dimensional tetrahedral elements. Interface surfaces were modeled between this component and the surrounding concrete to allow free tangential movement, with no strength in tension but large normal stiffness in compression to simulate the development of stresses in the concrete from the transverse deformations of the bars. The three-dimensional component also extended from the corbel face to the unbonded region of the brace; however, unlike the one-dimensional component, it was not connected to the bonded region, thus developing no axial stress. Within the end-gap region, each one-dimensional truss element node was embedded (constrained) within the surrounding steel three-dimensional tetrahedral elements, again assuming zero bond strength, to ensure that the one-dimensional line elements did not buckle during the multicyclic analyses.

Modeling of other brace reinforcement

The terminated longitudinal bars in the brace were modeled using one-dimensional truss elements with the same bilinear steel stress-strain relationship for the energy-dissipation bar elements (Fig. 5) and cyclic characteristics based on the Menegotto-Pinto model.[23] Each one-dimensional element

extended between the ends of the brace (without crossing the end gaps) using nodes embedded to the surrounding concrete to represent fully bonded conditions for the bars. As stated previously, design and modeling assumptions related to the effectiveness of bond in the brace should be evaluated experimentally in future research.

Transverse confinement reinforcement was modeled explicitly with the same one-dimensional truss elements used for the terminated longitudinal reinforcement. To reduce numerical complexity, the spirals were simplified into octagonal discrete hoops with identical spacing as the spirals, and the nodes of each hoop were embedded in the concrete.

Modeling of concrete

Concrete was modeled using three-dimensional 10-node quadratic tetrahedral elements. In all analyses, the end block and column regions (Fig. 4) were modeled using linear-elastic concrete material properties with a modulus of elasticity E_c of 4415 ksi (30,440 MPa) and a Poisson's ratio of 0.2. The modulus of elasticity was calculated based on ACI 318-19[24] for a design concrete compressive strength f'_c of 6 ksi (41 MPa).

To investigate the global buckling and multicyclic behavior of the brace, the brace concrete was modeled using a nonlinear fracture-plastic constitutive material model.[23] **Figure 7** shows the compression stress-strain law used for this concrete model, with the compressive strength f'_c of 6 ksi (41 MPa). The concrete behavior up to the peak stress was based on the default stress-strain curve[23] formulated from *fib*'s (International Federation for Structural Concrete's) *Model Code for Concrete Structures* (CEB-FIP Model Code 90)[31] with peak strength reached at a strain of 0.002. The concrete modulus of elasticity

E_c was calculated as 4415 ksi (30,440 MPa). After the peak stress, the softening law of the model has a linearly descending stress-strain relationship based on a Van Mier fictitious compression plane model, where the slope of the relationship depends on the size of the mesh element to minimize sensitivity of the analysis results to mesh size.

The tension behavior of the brace concrete before cracking was modeled as linearly elastic, with a tension strength f_t' of 0.581 ksi (4.01 MPa), which was calculated based on ACI 318-19 using f_c' of 6 ksi (41 MPa). The tension behavior after cracking was modeled using an exponential crack opening law in combination with the "crack band" theory. This law models the cracking behavior based on a user-defined concrete fracture energy G_f and critical crack opening width at complete release of stress w_c (Fig. 7). For the analyses described in this paper, G_f and w_c were taken as the default values[23] of 0.33 lb/in. (58 N/m) and 0.0197 in. (0.500 mm), respectively. Fully rotated cracks were assumed, allowing the cracks to change direction depending on varying principal stress directions under cyclic loading.

Simplifying assumptions

To justify the simplified boundary conditions of the isolated brace subassembly model in Fig. 4, the monotonic compression behavior of one brace was analyzed under different boundary conditions. These analyses investigated the brace behavior with and without additional beam and column elements and under different restraint conditions for the columns. To model the brace within a frame, beam and column components were connected to the existing end block and column (**Fig. 8**), thus creating a single-story model. The beam and column dimensions were modeled as 36 × 20 in. (910 × 510 mm) and 36 × 36 in. sections, respectively, with the centroid of each beam and column placed in line with the work-point nodes of the brace. All beams and columns were modeled using elastic three-dimensional 10-node quadratic

tetrahedral elements with a concrete modulus of elasticity E_c of 4415 ksi (30,440 MPa).

The results for brace axial force versus story drift in Fig. 8 show that, compared with the story model, the isolated brace subassembly model (without the added beam and column components) reached global buckling at a lower force and drift, indicating that the simplified model provides conservative results. This difference can be explained by the rotation of the story model allowing increased rotation of the bottom work-point node of the brace, which also increases the buckling load and delays failure of the brace. Based on these results, the analyses conducted in this study using the isolated brace subassembly model in Fig. 4 are considered to be conservative.

Another conservative simplification was made in modeling the local buckling of the energy-dissipation bars. Except for the analyses investigating closure of the brace end gaps, the end-gap regions were modeled with the assumption that the cover concrete on either side of the gap was ineffective in providing lateral support to the bars. This assumption was modeled by increasing the width of each end gap by the distance to the centerline of the first hoop in both the corbel and the brace. Effectively, this consideration increased the gap width by an amount equal to twice the concrete cover and a full hoop bar diameter. The analysis results described in the next section show that this conservative modeling assumption greatly influenced the buckling of the energy-dissipation bars in the end-gap regions. Future experimental work is necessary to determine whether this assumption should be adjusted.

Analysis results

This section provides the results from the analyses investigating brace behavior and selected failure modes. **Figure 9** shows an example of each undesirable failure mode discussed herein.
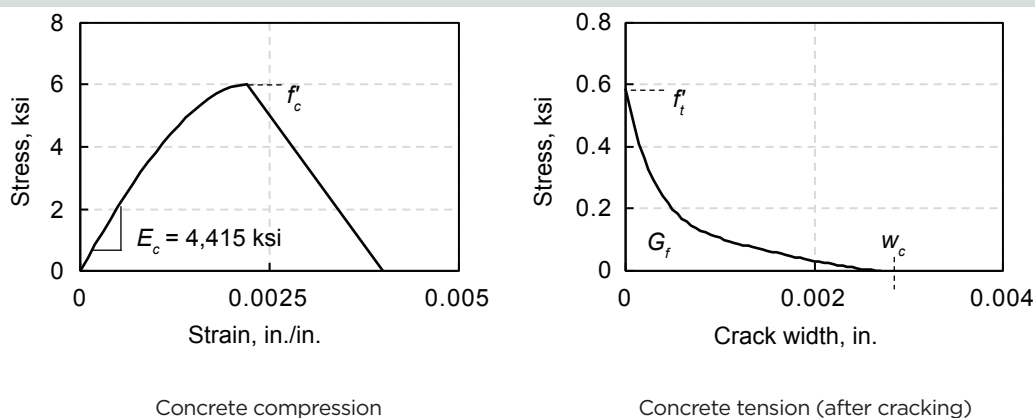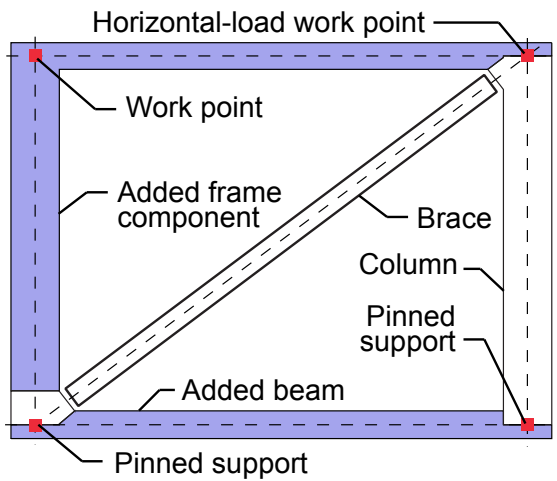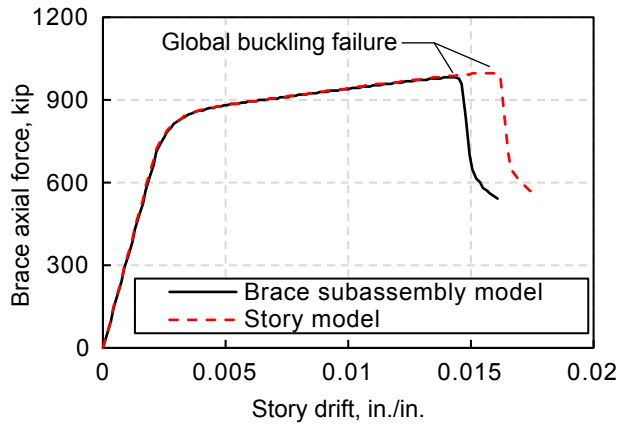

Figure 7. Stress-strain relationships for concrete in the finite element analysis modeling software. Note: E_c = concrete modulus of elasticity; f_c' = concrete compressive strength; f_t' = concrete tension strength; G_f = fracture energy of concrete; w_c = critical crack-opening width of concrete at complete release of stress. 1 in. = 25.4 mm; 1 ksi = 6.895 MPa.

Figure 8. Monotonic compression behavior of brace models with different boundary conditions (compression positive). Note: 1 in. = 25.4 mm; 1 ksi = 6.895 MPa.

Global buckling of the brace

Failure of a brace through global buckling can occur if the entire brace component buckles in compression (Fig. 9). Analyses of this failure mode aimed to determine the brace axial forces corresponding to global buckling under different brace conditions and to develop a design prediction for these axial forces.

Single-cyclic analyses of brace subassembly models were initially used to investigate global buckling. In these analyses, the brace model was first pulled (that is, the top work point of the brace in Fig. 4 was laterally loaded to the right), placing the brace in tension; then the load was reversed, placing the brace in compression.

This procedure allowed buckling to be evaluated after the brace had elongated and the energy-dissipation bars had yielded in tension, as compared with a monotonic compression analysis of the brace loaded from its original undeformed length. It was found that the lengthening of the brace and the widening of the gap regions in tension have an insignificant effect on the global buckling load of the brace. Consequently, all subsequent analyses of global buckling were conducted under monotonic compression loading for simplicity (that is, pushover analysis of the model toward the left in Fig. 4).

Three sets of brace configurations were evaluated under monotonic compression loading. The first set was designed using the aforementioned procedure (design set), whereas designs for the
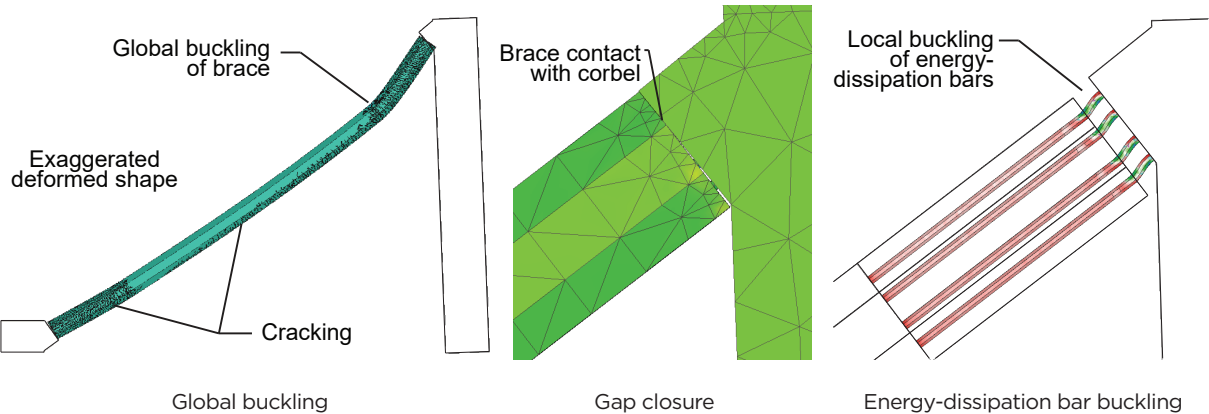

Figure 9. Simulated undesirable failure modes for braces in compression: global buckling of the brace, bearing of the brace on the adjacent corbel (gap closure), and translational buckling of the energy-dissipation bars across the gap region.

second and third sets were based on extreme brace configurations that deliberately induced global buckling, but are outside the likely range of practicality. Specifically, the second set (extreme set) investigated extreme brace conditions, such as long length and small section, and the third set (unbonded length set) focused on the unbonded length of the energy-dissipation bars with all other variables remaining constant. **Table 2** summarizes the characteristics of each brace configuration as well as the analysis results, namely, the brace axial force at global buckling P_{gb}.

Figure 10 presents the results for brace axial force versus story drift from the three sets of analyses. The results from the first set (braces designated A1 through A5 in Table 2) showed that braces within typical ranges of design are not susceptible to global buckling. This is because the maximum axial force that can be developed through the ultimate strength of the energy-dissipation bars remains less than the buckling force of a brace with a realistic length and energy-dissipation steel reinforcement ratio.

Table 2. Summary of global buckling analyses

Brace designation	A_g, in.²	I_g, in.⁴	Energy-dissipation bars		L, in.	Unbonded length, in.	P_{gb}, kip	K
			Total area, in.²	Ratio, %				
Design set								
A1*	331	8758		3.8	240	98		
A2*	212	3587		5.9	240	98		
A3	331	8758	12.5	3.8	240	98	No buckling	No buckling
A4*†	306	7816		4.1	240	98		
A5*	331	8758		3.8	420	160		
Extreme set								
B1	212	3587	12.5	5.9	420	160	919	0.98
B2	162	2103	12.5	7.7	400	148	786	0.85
B3†	210	3684	12.5	5.9	400	148	985	1.01
B4	212	3587	12.5	5.9	400	148	975	1.00
B5‡	212	3587	12.5	5.9	400	148	936	1.02
B6	212	3587	9.4	4.4	400	148	926	1.03
B7	212	3587	6.2	2.9	400	148	888	1.05
Unbonded length set								
C1						0	1377	0.84
C2						49	1173	0.91
C3						89	1077	0.95
C4	212	3587	12.5	5.9	400	111	1025	0.98
C5						148	966	1.01
C6						222	903	1.04
C7						400	893	1.05

Note: A_g = gross cross-sectional area of brace; I_g = gross cross-sectional moment of inertia of brace; K = effective length factor of brace (based on Euler elastic critical buckling load equation, calculated using concrete modulus of elasticity E_c of 4415 ksi, I_g, L, and P_{gb}); L = diagonal length of brace from corbel face to corbel face; P_{gb} = simulated brace axial force at global buckling. 1 in. = 25.4 mm; 1 kip = 4.448 kN; 1 ksi = 6.89 MPa.

*Grade 60 (414 MPa) steel was assumed in these cases. Grade 80 (552 MPa) steel was assumed in all other cases.

†Square section was used in these cases. Octagon section was used in all other cases.

‡Energy-dissipation bars in this case were arranged closer to the center of the brace section rather than against the spiral confinement as was assumed in every other case.

All configurations in the second set (braces B1 through B7 in Fig. 10) buckled globally into a similar shape (Fig. 9) with the largest brace deformations eventually concentrating at the ends of the bonded region. These analyses showed extensive cracking in the end regions of the brace, which was likely due to the buckling of the brace and lateral expansion of the energy-dissipation bars under compression. A similar buckled shape was also observed for all configurations in the third set (braces C1 through C7 in Fig. 10) except for the all-bonded (C1) and all-unbonded (C7) cases. Because these cases did not have transitions between the bonded and unbonded regions of the brace, the global buckling deformations were distributed over the entire brace without concentrating in any specific region. The results from the second and third analysis sets showed that the buckling force is influenced by a variety of parameters, including the placement of the energy-dissipation bars within the brace section, the size of the end gaps, and the ratio of unbonded to bonded lengths of the brace. However, the section size and length of the brace were found to have the greatest effect on the buckling force; thus, the subsequent discussion is focused on these variables.

For design predictions, the results from the second and third sets of analyses indicated that the equation for the Euler elastic critical buckling load P_{cr} can provide a reasonable estimate of the buckling force of the brace:

$$P_{cr} = \frac{\pi^2 E_c I_g}{(KL)^2}$$

where

I_g = gross cross-sectional moment of inertia of the brace

K = effective length factor of the brace

L = diagonal length of the brace from corbel face to corbel face

The global buckling failure demonstrated by the analyses was not elastic. Thus, the use of the Euler elastic buckling equation is only intended to be a simple design estimate rather than an accurate representation of the actual inelastic buckling of a brace. Similarly, the terms of the P_{cr} equation (such as the moment of inertia) and the reported values in Table 2 are based on the gross brace cross section (rather than the transformed section) and do not account for differences in the unbonded versus bonded regions of the brace.

A theoretical effective length factor K was calculated using the Euler elastic buckling equation together with the simulated buckling force P_{gb} of each brace (in the second and third sets of configurations) and the corresponding E_c, I_g, and L (Table 2 and **Fig. 11**). While some of the models resulted in a K value slightly greater than 1, no brace exceeded 5% of this value. Thus, a K value of 1 (corresponding to pin-pin boundary conditions) is recommended to provide a reasonable estimate of the brace buckling force for design.
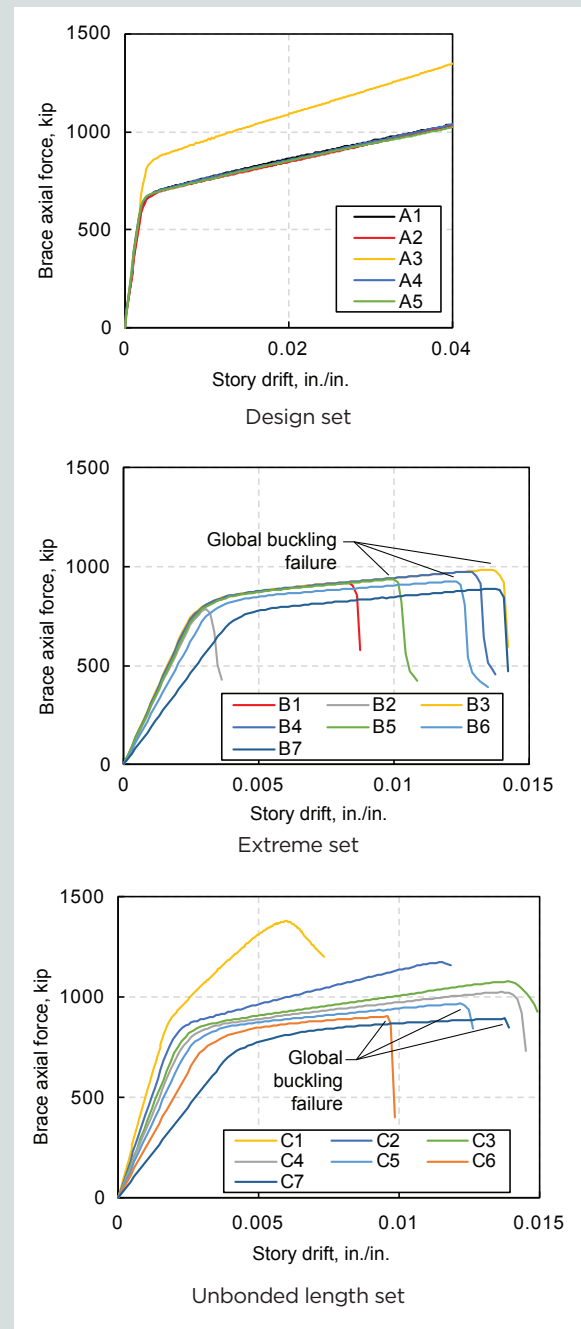

Figure 10. Brace axial force–versus–story drift behavior investigating global buckling (compression positive). Note: 1 in. = 25.4 mm; 1 kip = 4.448 kN.

Closure of the end gaps

Monotonic compression analyses were conducted to investigate brace failure through the closure of end gaps (Fig. 9). These analyses were done on models using the design width of the end gaps, without removing the concrete cover on the corbel and brace ends. The results indicated that braces designed using the aforementioned procedure were not susceptible to failure through gap closure. In these analyses, the brace deformations were near evenly distributed between the two end-gap regions.

In a real structure with asymmetries/imperfections, closure may occur at only one of the end gaps, while the other gap remains open. In this scenario, significant concrete damage is not expected because the forces that can be transferred through the closed end would be limited by the compression force of only the energy-dissipation bars (not the full brace section) at the open gap. In other words, both end gaps would need to be closed for larger compression forces to develop in the brace, which is prevented by designing a minimum total width for the two end gaps. Future experimental work should be conducted to investigate effects of asymmetries and imperfections on the brace behavior.

Translational buckling of the energy-dissipation bars

Failure of a brace can occur if the energy-dissipation bars buckle locally over their laterally unsupported length across the end-gap regions (Fig. 9). This buckling can occur through translational (lateral) as well as torsional deformations of the energy-dissipation bars; however, the study described herein did not include torsional buckling. In general, future experimental research is needed in this area because accurate numerical simulation of bar buckling is difficult.

Single-cyclic analyses using three-dimensional steel elements modeling the energy-dissipation bars were used to investigate this failure mode. As described previously, the end-gap regions were modeled with the conservative assumption that the cover concrete on either side of the gap is ineffective in providing lateral support to the bars. Brown and Kunnath[32] have shown that buckling of reinforcing bars under uniaxial loading is not expected to occur unless the unsupported length of the bar exceeds six times the bar diameter d_b. Initial results of the brace analyses conducted in this research showed that buckling of the energy-dissipation bars crossing the end gaps in a brace could occur even when the unsupported length is significantly shorter than $6d_b$.

To better understand the buckling of the energy-dissipation bars, axial compression analyses on groups of isolated bars with different lengths and boundary conditions were conducted (**Fig. 12**). The results indicated that this mode of failure is primarily driven by the inelastic buckling of the bars in combination with the specific boundary conditions of the bars across the gap regions in a brace. Because each end of the brace can translate laterally (that is, in a direction transverse to the bar axis) with respect to the adjacent corbel, the boundary conditions of the bars in the isolated analyses were represented as fixed at one end while free to translate but not rotate at the other end (fixed–transverse free configuration) (Fig. 12). These conditions differ from previous studies of bar buckling, where the bars were generally tested under assumed uniaxial loading conditions with no lateral translation allowed (fixed-fixed configuration). If the bars undergo lateral translation due to the lateral displacements of the brace with respect to the corbel, they can buckle over unsupported lengths much shorter than those for bars that are prevented from translation.
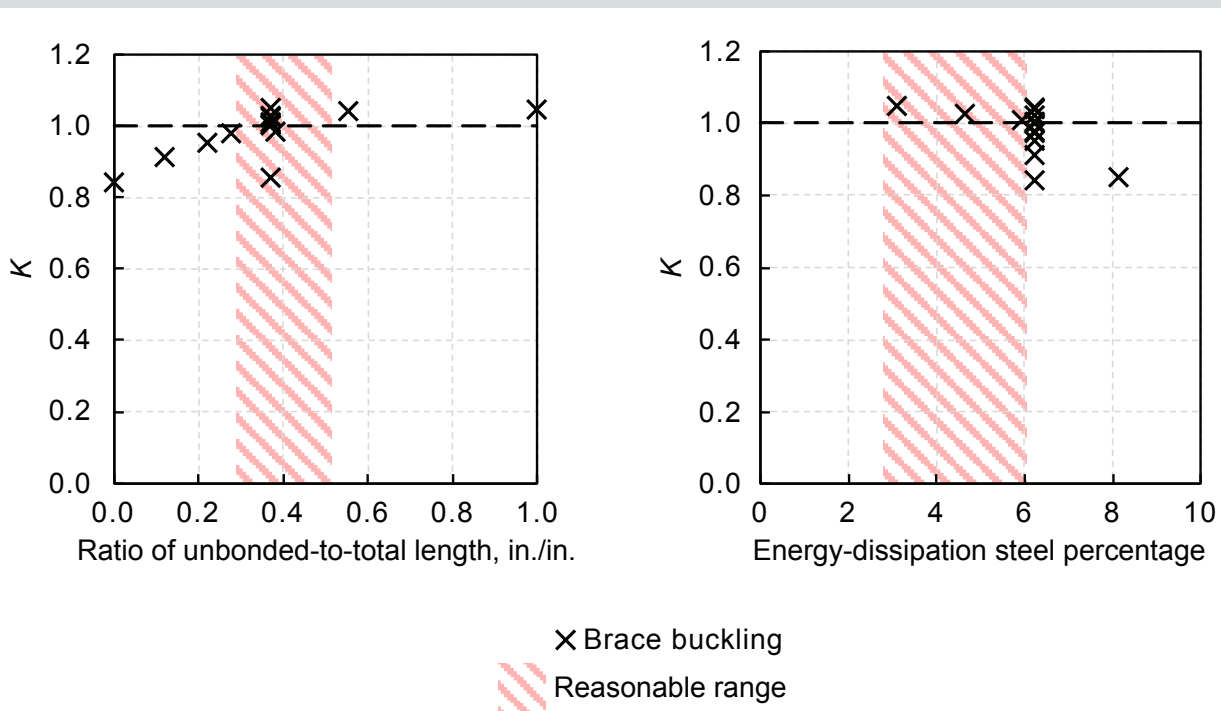

Figure 11. Theoretical effective length factor K based on the Euler elastic critical buckling load equation. The ranges of values considered reasonable for the unbonded-to-total brace length ratio and energy-dissipation steel percentage are marked on the graphs. Note: 1 in. = 25.4 mm.

The isolated bar-buckling analyses were conducted with increasing bar lengths until buckling occurred under both fixed–transverse free and fixed-fixed boundary conditions. The bars with the fixed-fixed configuration began to develop buckling at lengths around $6d_b$, matching the results reported by Brown and Kunnath.[32] When relative lateral translation of the bars was allowed, buckling began to develop at unsupported lengths of approximately $3d_b$. This result is consistent with the idea that the fixed–tansverse free configuration is theoretically equivalent to one-half of the corresponding fixed-fixed configuration (with length double that of the fixed–transverse free configuration).

The maximum unsupported length of $3d_b$ to prevent buckling of the energy-dissipation bars may be too small to prevent potential failure of the brace through end-gap closure, especially if the cover concrete on either side of the gap in a brace is assumed to be ineffective in providing lateral support to the bars. Therefore, a potential method for preventing lateral translation of the bars using an axially decoupled steel shear dowel across each end gap was investigated. These shear dowels were embedded and bonded to the beam and column corbel regions and extended into the brace section but were axially debonded from the surrounding concrete by wrapping the length of the dowel inside the brace, with an open pocket allowing axial movement at one end of the dowel (**Fig. 13**). In this arrangement, the dowels are intended to prevent the energy-dissipation bars from laterally translating, without contributing to the axial behavior of the brace.

Several braces were modeled with different dowel variations. Finite element models with appropriately sized shear dowels to prevent lateral translation across the end gaps no longer exhibited translational buckling of the energy-dissipation bars. Based on these findings, a simple procedure was developed to design the shear dowels.

The shear force demand across the end gaps was found to vary widely and was difficult to predict accurately without a numerical model in a practical design scenario. Therefore, the dowel was sized to provide a percentage of the total shear stiffness of the energy-dissipation bars instead of being based on the shear force demand. Specifically, the models indicated that steel dowels providing a shear stiffness equal to about 50% of the shear stiffness from the energy-dissipation bars may be sufficient in preventing the translational buckling of bars with unsupported lengths up to about six times the bar diameter d_b. Because shear stiffness is proportional to the shear area, the steel dowel must therefore have an area equal to about 50% of the total area of the energy-dissipation bars crossing the end gap.

Importantly, the finite element analyses showed that the simulation of bar buckling is particularly sensitive to numer-
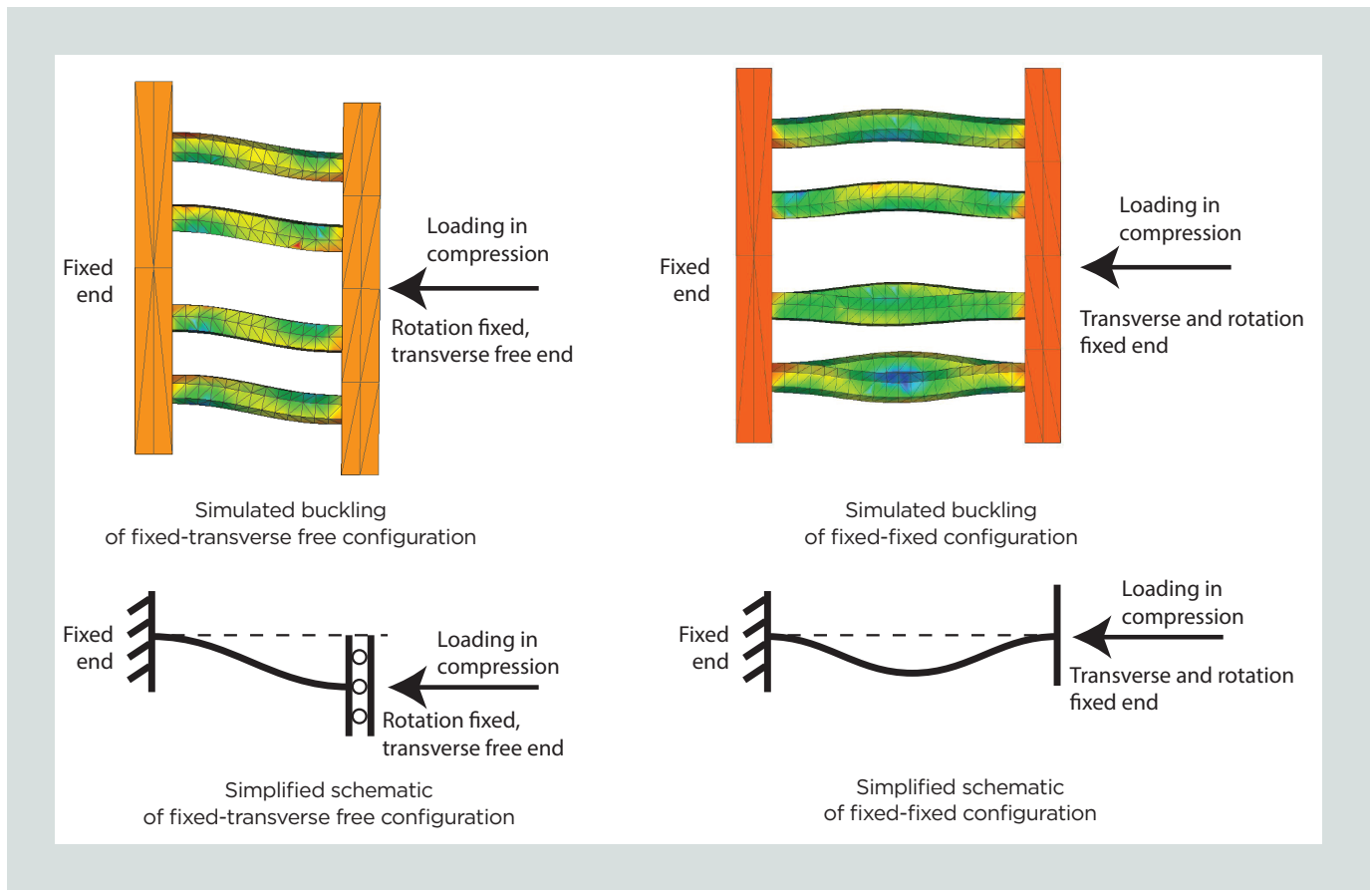

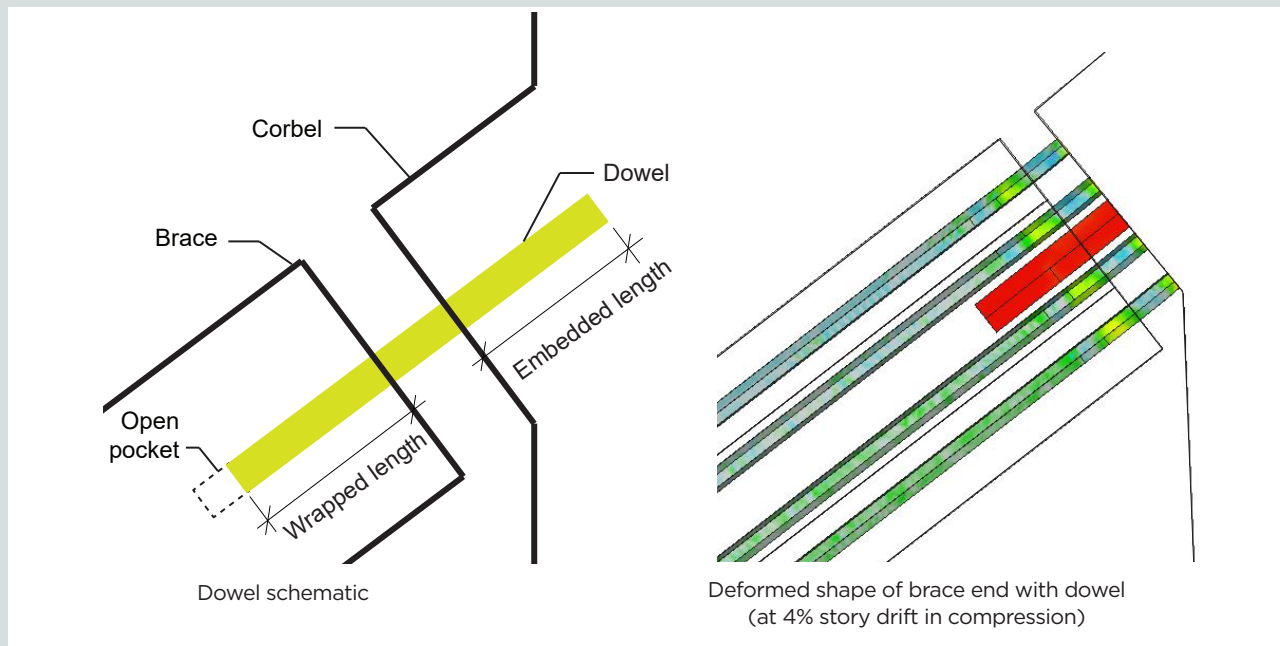**Figure 12.** Isolated energy-dissipation bar buckling simulated with lateral translation.

Figure 13. Axially decoupled shear dowel and simulated effect.

(Dowel schematic labels: Corbel, Dowel, Brace, Embedded length, Open pocket, Wrapped length)

Dowel schematic

Deformed shape of brace end with dowel
(at 4% story drift in compression)

ical model details such as the mesh size. Future experimental research should evaluate the effects of the dowel, different dowel sectional areas and shapes, and the number of dowels needed across each end gap. The dowel shape and number of dowels across each end gap may be dictated by torsional buckling of the energy-dissipation bars, which could not be modeled numerically within the scope of this research.

Desired behavior up to ductile low-cycle fatigue fracture of the energy-dissipation bars

The desired failure mode for the proposed reinforced-concrete brace is ductile low-cycle fatigue fracture of the energy-dissipation bars within the unbonded regions, without buckling or end-gap closure. The behavior of such a ductile brace was investigated through multicyclic analyses. Because the analyses in this research could not explicitly model low-cycle fatigue fracture, a limit for $\varepsilon_{s,max}$ of 0.06 was taken as the maximum usable tensile strain for the energy-dissipation bars based on experimental results from Aragon et al.[30]

Two loading sequences were used for the multicyclic analyses. The first sequence began with the first cycle at 0.1% story drift, with the story drift of each subsequent cycle increased by a factor of 1.5. The top graph in **Figure 14** shows the axial force–versus–story drift behavior of a ductile brace under this loading sequence, with the last point of the hysteretic plot representing when the energy-dissipation bars reach the maximum strain limit of 0.06. Cracking in the brace occurred in the middle bonded region, with stable behavior of the brace during load reversals in tension and compression. Cracking of the concrete led to a slightly smaller stiffness of the brace in tension versus

in compression. As targeted in design, the cyclic analyses under this sequence indicated that properly designed braces will fail due to ductile low-cycle fatigue fracture of the energy-dissipation bars around the maximum design story drift (4% drift for the braces discussed in this paper). However, because these results are based on the assumption that the energy-dissipation bars are viable up to 0.06 strain in tension, future experimental work is needed to determine the maximum strain limit of the bars under the specific deformation demands within a brace.

The second loading sequence followed the procedure prescribed for the cyclic qualification testing of steel buckling-restrained braces (AISC 341-16[33]). This loading sequence does not necessarily reach the maximum strain limit of the bars; rather, it focuses on testing the cumulative ductility of the brace at lower story drift values. The sequence was used in this investigation to demonstrate that well-designed concrete buckling-restrained braces can meet the deformation requirements currently prescribed for steel braces. The bottom graph in Figure 14 shows the axial force–versus–story drift behavior of the same concrete brace under the second loading sequence. Similar to the first sequence, cracking in the middle bonded region of the brace was stable throughout the analysis, with a slightly smaller stiffness of the brace in tension than in compression.

While the results of this analysis demonstrated that the concrete brace is viable under the requirements for steel braces, the current models do not explicitly account for the cumulative strain capacity of the energy-dissipation bars. Based on the experimental results from Aragon et al.,[30] the cumulative strain capacity of the bars is not expected to be reached before the maximum useable strain limit $\varepsilon_{s,max}$ of 0.06. However, further experimental work is
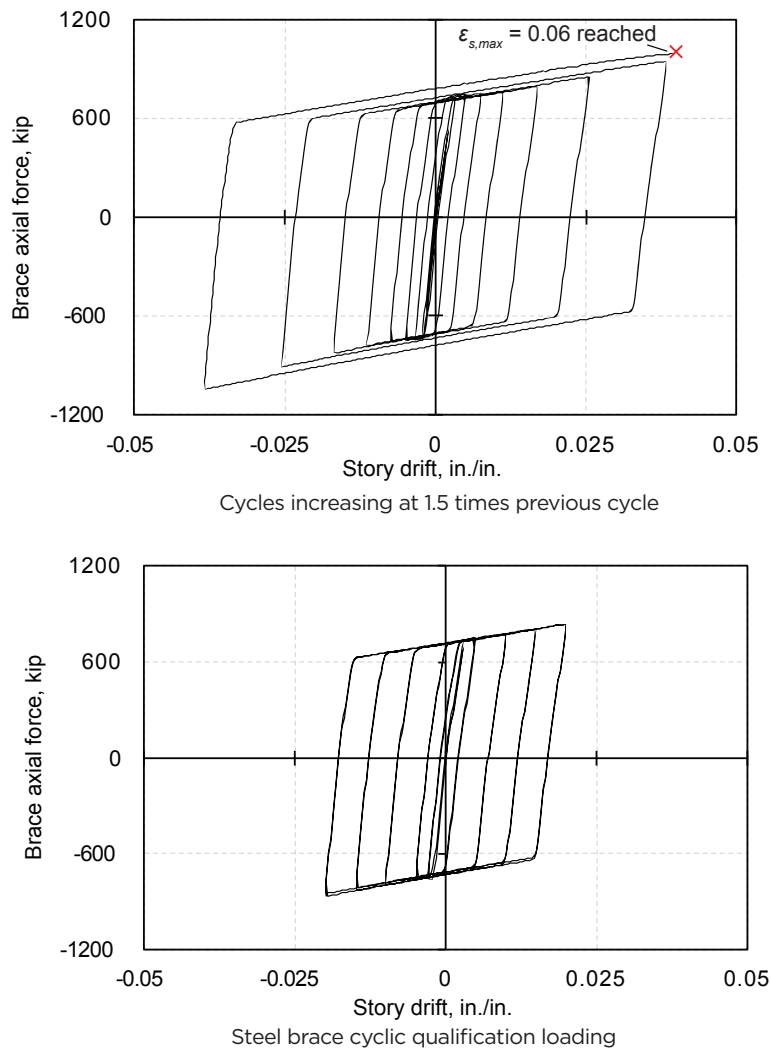
Figure 14. Simulated cyclic behavior of a well-designed brace with story drift increasing at 1.5 times the previous drift and under the AISC 341-16 cyclic qualification testing protocol for steel braces (tension positive, compression negative). Note: $\varepsilon_{s,max}$ = design usable tensile strain limit of energy-dissipation bars. 1 in. = 25.4 mm; 1 kip = 4.448 kN.

needed to determine the cumulative strain capacity of these bars under the specific deformation demands within a brace.

Conclusion

This study introduced a novel reinforced concrete buck-ling-restrained brace component and numerically evaluated its seismic design and behavior. A design procedure was developed to achieve ductile behavior of the brace under reversed cyclic loading. Nonlinear finite element analyses were conducted to investigate some of the potential failure modes, including global buckling of the brace, closure of end gaps, and translational buckling of the energy-dissipation bars, as well as the desired behavior of a well-designed brace up to ductile low-cycle fatigue fracture of the energy-dissipation bars. These analyses included monotonic compression, single-cy-clic, and multicyclic loading of isolated brace subassemblies within a diagonal orientation.

The conclusions from the study may be limited to the brace configurations analyzed, assumptions made, and limitations of the finite element modeling software.

• Failure of the brace through global buckling is unlikely for practical brace designs. Susceptibility to this failure mode can be determined through the calculation of the Euler elastic critical buckling load with an effective length factor *K* of 1, gross cross-sectional moment of inertia of the brace, length of the brace from corbel face to corbel face, and concrete modulus of elasticity.

• Closure of the end gaps at the maximum design story drift can be prevented using the design procedure described in this paper.

• Local buckling of the energy-dissipation bars across the end gaps is a critical failure mode that can limit the duc-

tility capacity of the brace in compression. If the bars are allowed to undergo lateral translation due to transverse displacements of the brace with respect to the corbels, they can buckle at unsupported lengths of approximately three times the bar diameter.

• Although the end-gap width can be reduced to prevent buckling of the energy-dissipation bars, this can lead to closure of the end gaps, triggering other undesirable damage and failure modes prior to the maximum design story drift of the brace in compression.

• Alternatively, an axially decoupled steel shear dowel with an area equal to about 50% of the total area of the energy-dissipation bars can be used across each end gap to prevent lateral translation of the bars and allow longer unsupported lengths up to about six times the bar diameter.

The results from the analyses presented herein have not yet been validated with experimental data. Experimental research is needed to investigate the assumptions used in these analyses, validate the design and behavior of the brace, and provide further research basis for the use of the proposed brace. The specific topics recommended for experimental research include the following:

• development of longitudinal reinforcement within the bonded regions of the brace

• design and detailing of the corbels and other regions of beams and columns adjacent to the brace

• translational and torsional buckling of the energy-dissipation bars across the end gaps, including the need and design of dowels to prevent this buckling

• low-cycle fatigue and cumulative strain capacity of the energy-dissipation bars

• design of confinement reinforcement

• brace cross section and maximum longitudinal reinforcement ratio

• area of terminated reinforcement

• effects of construction asymmetries and imperfections on brace behavior

• post-earthquake repair or replacement of the brace

In addition to experiments involving isolated braces and braced-frame subassemblies, experiments on multistory frames and braced-frame buildings are necessary before the proposed brace can be used in practice. Tests should investigate different brace configurations, such as chevron and single-diagonal arrangements. The numerical study described in this paper focused on the behavior of isolated single-brace subassemblies. Future numerical work should consider the behavior, seismic performance, and resilience of the brace within its intended precast concrete frame story unit as well as in complete multistory braced-frame structures. Ultimately, this additional research will provide a more complete understanding of this novel brace and may provide justification for its use within a seismic-resisting building frame.

Acknowledgments

References

1. Watanabe, A., Y. Hitomi, E. Saeki, A. Wada, and M. Fujimoto. 1988. "Properties of Brace Encased in Buckling-Restraining Concrete and Steel Tube." In *Proceedings of the 9th World Conference on Earthquake Engineering* 4: 719–724. https://www.iitk.ac.in/nicee /wcee/article/9_vol4_719.pdf.

2. Tremblay, R., G. Degrange, and J. Blouin. 1999. "Seismic Rehabilitation of a Four-Storey Building with a Stiffened Bracing System." In *Proceedings of the 8th Canadian Conference on Earthquake Engineering*, 549–554. Vancouver, BC, Canada: Canadian Association for Earthquake Engineering.

3. Merritt, S., C. M. Uang, and G. Benzoni. 2003. *Subassemblage Testing of CoreBrace Buckling-Restrained Braces*. Structural Systems Research Project report TR-2003/04. La Jolla, CA: University of California San Diego.

4. Black, C. J., N. Makris, and I. D. Aiken. 2004. "Component Testing, Seismic Evaluation and Characterization of Buckling-Restrained Braces." *Journal of Structural Engineering* 130 (6): 880–894. https://doi .org/10.1061/(ASCE)0733-9445(2004)130:6(880).

5. Andrews, B. M., L. A. Fahnestock, and J. Song. 2009. "Ductility Capacity Models for Buckling-Restrained Braces." *Journal of Constructional Steel Research* 65: 1712–1720. https://doi.org/10.1016/j.jcsr.2009.02.007.

6. Clark, P., I. D. Aiken, E. Ko, K. Kasai, and I. Kimura. 1999. "Design Procedures for Buildings Incorporating Hysteretic Damping Devices." In *Proceedings of the 68th Annual Convention of the Structural Engineers Association of California*, 355–371. Sacramento, CA: SEAOC (Structural Engineers Association of California).

7. Clark, P., K. Kasai, I. D. Aiken, and I. Kimura. 2000. "Evaluation of Design Methodologies for Structures Incorporating Steel Unbonded Braces for Energy Dissipation." In *Proceedings of the 12th World Conference on Earthquake Engineering*. Upper Hutt, NZ: New Zealand Society for Earthquake Engineering. https://www.iitk.ac.in/nicee/wcee/article/2240.pdf.

8. Sabelli, R., S. Mahin, and C. Chang. 2003. "Seismic Demands on Steel Braced-Frame Buildings with Buckling-Restrained Braces." *Engineering Structures* 25 (5): 655–666. https://doi.org/10.1016/S0141-0296 (02)00175-X.

9. AISC (American Institute of Steel Construction) and SEAOC. 2001. *Recommended Provisions for Buckling-Restrained Braced Frames*. Chicago, IL: AISC.

10. ASCE (American Society of Civil Engineers) and SEI (Structural Engineering Institute). 2005. *Minimum Design Loads for Buildings and Other Structures*. ASCE/SEI 7-05. Reston, VA: ASCE.

11. Dangol, I., D. Thapa, and C. P. Pantelides. 2022. "Experimental Evaluation of Post-tensioned Bridge Bent under Cyclic Loads and Comparison to Hybrid Bridge Bents." *Engineering Structures* 256: 113962. https://doi.org/10.1016/j.engstruct.2022.113962.

12. Dangol, I., and C. P. Pantelides. 2022. "Resilient Posttensioned Bridge Bent with Buckling Restrained Brace." *Journal of Bridge Engineering* 27 (2): 04021107. https://doi.org/10.1061/(ASCE)BE.1943-5592.0001823.

13. El-Bahey, S., and M. Bruneau. 2011. "Buckling Restrained Braces as Structural Fuses for the Seismic Retrofit of Reinforced Concrete Bridge Bents." *Engineering Structures* 33 (3): 1052–1061. https://doi.org/10.1016/j.engstruct.2010.12.027.

14. Wang, Y., L. Ibarra, and C. Pantelides. 2016. "Seismic Retrofit of a Three-Span RC Bridge with Buckling-Restrained Braces." *Journal of Bridge Engineering* 21 (11): 04016073. https://doi.org/10.1061/(ASCE)BE.1943-5592.0000937.

15. Viano, J. D., and T. C. Schaeffer. 2017. "Novel Use of Buckling-Restrained Braces in Precast Concrete Frames." *PCI Journal* 62 (5): 28–34. https://doi.org/10.15554/pcij62.5-03.

16. Guerrero, H, T. Ji, J. A. Escobar, and A. Teran-Gilmore. 2018. "Effects of Buckling-Restrained Braces on Reinforced Concrete Precast Models Subjected to Shaking Table Excitation." *Engineering Structures* 163: 294–310. https://doi.org/10.1016/j.engstruct.2018.02.055.

17. Oh, S., Y. C. Kurama, J. Mohle, and B. W. Saxey. 2021. "Seismic Design and Analysis of Precast Concrete Buckling-Restrained Braced Frames." *PCI Journal* 66 (5): 54–83. https://doi.org/10.15554/pcij66.5-03.

18. FEMA (Federal Emergency Management Agency). 2009. *Quantification of Building Seismic Performance Factors*. FEMA P-695. Washington, DC: FEMA.

19. Mazzoni, S., F. McKenna, M. H. Scott, and G. L. Fenves. 2006. *OpenSees Command Language Manual*. Berkeley: Pacific Earthquake Engineering Research Center, University of California, Berkeley. https://opensees.berkeley.edu/OpenSees/manuals/usermanual/OpenSeesCommandLanguageManualJune2006.pdf.

20. Kessler, H. 2021. "Initial Investigation of Connection Behavior for Buckling-Restrained Braces (BRBs) in Precast Concrete Frames." MS thesis, Clemson University, Clemson, SC.

21. AISC. 2017. *Steel Construction Manual*. 15th ed. Chicago, IL: AISC.

22. ASTM Subcommittee A01.05. 2016. *Standard Specification for Deformed and Plain Low-Alloy Steel Bars for Concrete Reinforcement*. ASTM A706/A706M. West Conshohocken, PA: ASTM International.

23. Cervenka, V., J. Cervenka, and R. Pukl. 2002. "ATENA—A Tool for Engineering Analysis of Fracture in Concrete." *Sadhana* 27 (4): 485–492. https://doi.org/10.1007/BF02706996.

24. ACI (American Concrete Institute) Committee 318. 2019. *Building Code Requirements for Structural Concrete (ACI 318-19) and Commentary (ACI 318R-19)*. Farmington Hills, MI: ACI.

25. Kurama, Y., S. Sritharan, R. Fleischman, J. Restrepo, R. Henry, N. Cleland, S. K. Ghosh, and P. Bonelli. 2018. "Seismic-Resistant Precast Concrete Structures: State of the Art." *Journal of Structural Engineering* 144 (4): 03118001. https://doi.org/10.1061/(ASCE)ST.1943-541X.0001972.

26. Smith, B. J., and Y. C. Kurama. 2014. "Seismic Design Guidelines for Solid and Perforated Hybrid Precast Concrete Shear Walls." *PCI Journal* 59 (3): 43–59. https://doi.org/10.15554/pcij.06012014.43.59.

27. ASCE and SEI. 2022. *Minimum Design Loads and Associated Criteria for Buildings and Other Structures*.

ASCE/SEI 7-22. Reston, VA: ASCE. https://doi.org /10.1061/9780784415788.

28. AISC. 2018. *Seismic Design Manual*, 3rd ed. Chicago, IL: AISC.

29. Kersting, R. A., L. A. Fahnestock, and W. A. López. 2015. *Seismic Design of Steel Buckling-Restrained Braced Frames: A Guide for Practicing Engineers*. National Earthquake Hazards Reduction Program Seismic Design technical brief 11. Gaithersburg, MD: National Institute of Standards and Technology. https:// doi.org/10.6028/NIST.GCR.15-917-34.

30. Aragon, T. A., Y. C. Kurama, and D. F. Meinheit. 2020. "Behavior of Ductile Short-Grouted Seismic Reinforcing Bar-to-Foundation Connections Under Adverse Construction Conditions." *PCI Journal* 65 (4): 33–50. https://doi.org/10.15554/pcij65.4-01.

31. *fib* (International Federation for Structural Concrete). 1990. *Model Code for Concrete Structures*. CEB-FIP Model Code 90. London, UK: Thomas Telford Ltd.

32. Brown, J., and S. Kunnath. 2004. "Low-Cycle Fatigue Failure of Reinforcing Steel Bars." *ACI Materials Journal* 101 (6): 457–466. https://doi.org/10.14359/13484.

33. ANSI and AISC. 2016. *Seismic Provisions for Structural Steel Buildings*. ANSI/AISC 341-16. Chicago, IL: AISC.

Notation

$A_{b,min}$ = minimum required area of energy-dissipation bars

A_g = gross cross-sectional area of brace

d_b = diameter of single energy-dissipation bar

E_c = concrete modulus of elasticity

E_s = energy-dissipation bar modulus of elasticity

E_{sh} = energy-dissipation bar postyield strain-hardening modulus

f'_c = concrete compressive strength

f'_t = concrete tension strength

$f_{y,min}$ = lowest expected yield strength of energy-dissipation bar

G_f = concrete fracture energy

h = work point–to–work point height of brace

I_g = gross cross-sectional moment of inertia of brace

K = effective length factor of brace

L = diagonal length of brace measured from corbel face to corbel face

ℓ_b = work point–to–work point diagonal length of brace

$\ell_{unb,min}$ = minimum unbonded length at each end of brace

N_u = factored design axial force of brace

P_{cr} = Euler elastic critical buckling load

P_{gb} = simulated brace axial force at global buckling

R = seismic response modification coefficient per ASCE 7-22

w = work point–to–work point horizontal length of brace

w_c = critical crack-opening width of concrete at complete release of stress

$w_{g,min}$ = minimum width of each end gap

Δ_b = change in brace length at maximum design story drift

$\Delta_{d,max}$ = maximum design story drift

ε_s = steel strain

$\varepsilon_{s,max}$ = design usable tensile strain limit of energy-dissipation bars

σ_s = steel stress

ϕ = capacity reduction factor for axial strength design of brace (taken as 0.9)

About the authors

Shane Oh is a PhD candidate in the Department of Civil and Environmental Engineering and Earth Sciences at the University of Notre Dame in Notre Dame, Ind.

Yahya C. Kurama, PhD, PE, is a professor in the Department of Civil and Environmental Engineering and Earth Sciences at the University of Notre Dame.

Jon Mohle, SE, is a senior product and market manager at Clark Pacific in Sacramento, Calif.

Lily Polster is a graduate student in the Department of Civil and Environmental Engineering and Earth Sciences at the University of Notre Dame.

Mark Manning, PhD, is a research scientist in the Department of Civil and Environmental Engineering and Earth Sciences at the University of Notre Dame.

Brad D. Weldon, PhD, is a teaching professor in the Department of Civil and Environmental Engineering and Earth Sciences at the University of Notre Dame.

Abstract

This paper describes a numerical investigation on the seismic design and behavior of a novel reinforced-concrete buckling-restrained brace component for use in precast concrete lateral-load-resisting frames. The design procedure aimed to develop a brace with ductile behavior under reversed cyclic loading. Nonlinear finite element analyses were conducted to investigate the following potential undesirable failure modes of the brace: global buckling of the brace, closure of the end gaps, and local translational buckling of the energy-dissipation bars. The results indicated that failure through global buckling is unlikely for practical brace designs. Closure of the end gaps can be prevented by designing a wide-enough gap at each end of the brace, but design must also ensure that local buckling of the energy-dissipation bars does not occur over their unsupported length across the end gaps. An axially decoupled steel shear dowel can be used to permit a wider end gap without triggering translational buckling of the energy-dissipation bars. Braces that are designed to prevent undesirable failure modes can provide stable behavior up to ductile low-cycle fatigue fracture of the energy-dissipation bars.

Keywords

Review policy

This paper was reviewed in accordance with the Precast/Prestressed Concrete Institute's peer-review process. The Precast/Prestressed Concrete Institute is not responsible for statements made by authors of papers in *PCI Journal*. No payment is offered.

Publishing details

Reader comments

Please address any reader comments to *PCI Journal* editor-in-chief Tom Klemens at tklemens@pci.org or Precast/Prestressed Concrete Institute, c/o *PCI Journal*, 8770 W. Bryn Mawr Ave., Suite 1150, Chicago, IL 60631. ⌡